Journal of Nuclear Materials 383 (2009) 247–253

Contents lists available at ScienceDirect

Journal of Nuclear Materials

journal homepage: www.elsevier.com/locate/jnucmat

Comparative study of predictive FE methods for mechanical properties of nuclear composites

Joshim Ali [a,*], Johar K. Farooqi [b], Derek Buckthorpe [a], Allister Cheyne [a], Paul Mummery [b]

[a] AMEC, Booths Park, Chelford Road, Knutsford, Cheshire WA16 8QZ, UK
[b] School of Materials, University of Manchester, Grosvenor Street, Manchester M1 7HS, UK

ARTICLE INFO

Article history:
Received 14 June 2008
Accepted 18 September 2008

ABSTRACT

Carbon fiber reinforced carbon (C/C) composites are candidate materials for plasma facing components in experimental fusion reactors such as: the ITER; the JT-60 – a Tokamak fusion test facility (JAEA); and for control rods in the next generation fission reactors. Therefore, determining their thermo-mechanical properties under irradiation is essential for safe design-cum-operation of future reactors. Development of reliable models which can predict such materials' behavior is of massive advantage against the conventional experimental verification which is hugely expensive and time-consuming. Three-dimensional finite element (FE) methods are used here for predicting Young's modulus of two woven C/C composites where tensile tests are performed for validation. Stress distribution results indicate that a novel image-based route for FE meshes compared to a unit cell approach gives stronger agreement with experimental data. The image-based approach captures true porosity as fine microstructural details are converted from X-ray tomographic data. In comparison, the unit cell model represents idealizations of composite architecture that ignores porosities.

1. Introduction

In the literature, numerous models have been reported that describe the behavior of composites [1–4]. These models are mainly based on meshes that have been manually or digitally created, e.g., the unit cell approach. These necessarily assume that the material can be represented reliably by an infinitely, repeating ideal structure. This is unlikely to be absolutely true for materials such as woven composites that have complex architectures with difficult and complicated fabrication processes.

The main advantages of finite element (FE) approaches compared to other numerical analysis methods are that: it is applicable to any field problem; it has no limitations on geometry, shape, boundary conditions or loading; many different parts and components can be combined; the material properties are not just restricted to isotropy; and it can closely represent the actual material with the potential to easily improve the approximation by upgrading the mesh, e.g., enhancing features through increase of number of elements. Points to be cautious about are: (1) it is complicated, (2) time-consuming and (3) initially unreliable as it is possible to carry out complete FE analyses with little background knowledge of the method [5,6].

The aim of the current study is to show the potential of reliable FE models for advanced reinforced composite structures. This is done by comparing two different approaches for modeling woven composites. The first is a unique method that uses an image-based route in acquiring FE meshes [7]. This is achieved by combining X-ray microtomography (XMT) [8,9], which gives a high resolution image of the microstructure in 3D, with FE software codes [10,11]. Here the 'real' structure is converted directly into a 3D FE mesh. The development of this novel image-based approach has been presented elsewhere [7,12]. Somewhat similar approaches have also been adopted in literature for modeling polyurethane foams [13], cellular structures [14], graphite [15], alumina coatings [16], trabecular bone [17], dental structures [18] and metal matrix composites [19]. The second method used here is a 3D unit cell model of the structure [1,2], based on idealizations of the composite architecture through a plane-symmetric volumetric representative region. This model assumes that the material can be represented reliably by an infinitely repeating ideal structure modeled with a unit cell.

In this paper, the Young's moduli of two 2D woven C/C composites are predicted through FE analyses employed on both of these model types. The predictions are compared with experimental data for validation.

2. Composite material

Two-dimensional woven C/C composites in two heat-treated conditions were studied. These were graphitised and un-graphitised samples manufactured by Toyo Tanso, Japan (CX-270 grade).

---

[*] Corresponding author. Tel.: +44 1565 684 838; fax: +44 1565 684 870.
E-mail address: Joshim.Ali@Amec.com (J. Ali).

0022-3115/$ - see front matter © 2008 Elsevier B.V. All rights reserved.
doi:10.1016/j.jnucmat.2008.09.020

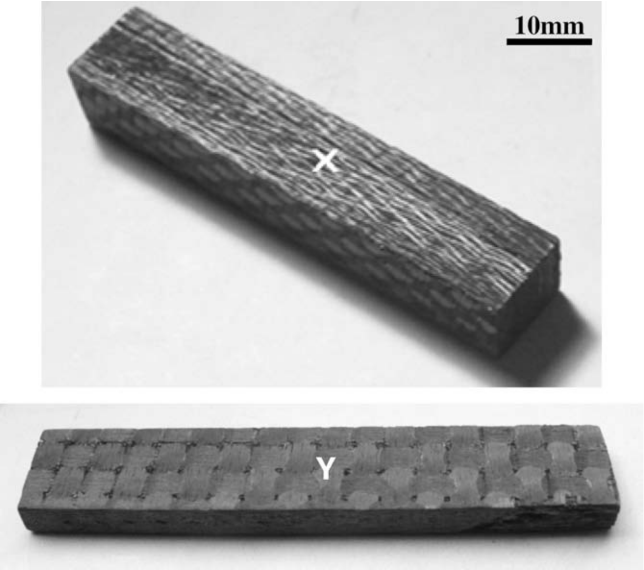

Fig. 1. C/C composite materials used in the current study.

The macroscopic architectures of both composites are shown in Fig. 1. These composites have two distinguishable sides: a lamina side '*X*' in which the fiber tows are both longitudinal and transverse in this orientation, and a perpendicular-to-lamina side '*Y*' in which they are all transverse.

Both composites were produced by impregnation of woven fiber reinforcements within a resin matrix precursor. The pitch-based carbon fibers were initially manufactured by melt spinning, and arranged in a simple plain weave. Following compaction and carbonization, isothermal chemical vapor deposition (CVD) was used to infiltrate carbon bearing gas into the interstices (gaps) between the arrays of fibers, while the graphitised composites were further processed at higher graphitization temperatures exceeding 1800 °C. The final composite microstructures comprised of three phases: woven pitch fibers, a graphitic matrix and pores.

3. Modeling

3.1. Image-based modeling approach

The method used to create 3D image-based FE meshes of the composites has been described in detail elsewhere [7,12]. These meshes were created directly from X-ray tomographic data using Simpleware® Ltd. (Innovation Centre, Exeter, UK) [10]. The imaging conditions used to scan the samples using the X-Tek HMX-225 laboratory X-ray microtomography kit [9] are shown in Table 1. Furthermore, a pixel size of ~10 μm has been chosen in order to generate reliable meshed volumes.

Table 1
Computed tomographic (CT) imaging parameters used to scan the composites are given here

X-ray tube: energy/intensity		Radiograph acquisition[a]			Volume reconstruction	
Voltage (kV)	Current (mA)	Angular displacement (°)	Exposure time (ms)	Frames per angular movement	Pixel size (μm)	Reconstructed volume (voxels)
35	0.25	0.3	160	32	10	768 × 768 × 523/597

[a] About 0.25 mm aluminum filter was also used during scanning to reduce noise effects in acquired radiographs.

The image-based meshes were cropped to a smaller size consisting typically of ~2 000 000 elements that were 8-node cubic linear brick C3D8 (first-order 3D elements) [11]. This volume restriction was due to limitations in computational power (based on the modeling resource of ABAQUS CAE v6.6 EF-1 using Windows 64 bit with 32GB RAM on eight cores). These meshes represented ~2.5 × 2.5 × 2.5 mm of the composite materials (Fig. 2). This volume was estimated from optical micrographs of the composite microstructures (Fig. 3).

A representative unit cell of the plain weave architecture has been identified in Fig. 4. This unit cell volume represented ~0.5 × 2 × 2 mm of the composite material, also estimated from optical micrographs. Care was taken to ensure that the meshes were cropped to such smaller regions that were still representative of the composite architectures, using this unit cell volume as a guiding minimum benchmark.

These image-based FE meshes are a significant improvement to the models previously published [7]. The major advantage of this modeling technique over conventional unit cell approach is that it accounts for true porosity in its models, since the real structure is converted directly into a 3D FE mesh.

The cropped image-based meshes of the composites in Fig. 2 are slightly larger volumes than the representative unit cell (Fig. 4).

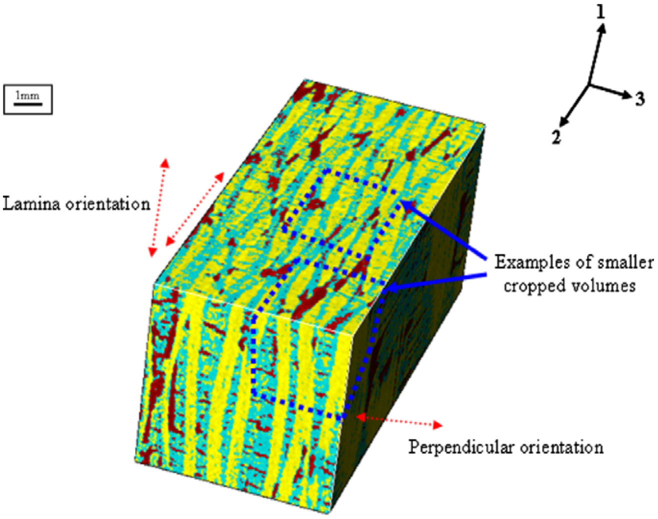

Fig. 2. Image-based FE meshes of the 2D C/C composite (graphitised), black elements = porosity, light grey = fibers and matrix in direction 1 and dark grey = fibers and matrix in direction 2.

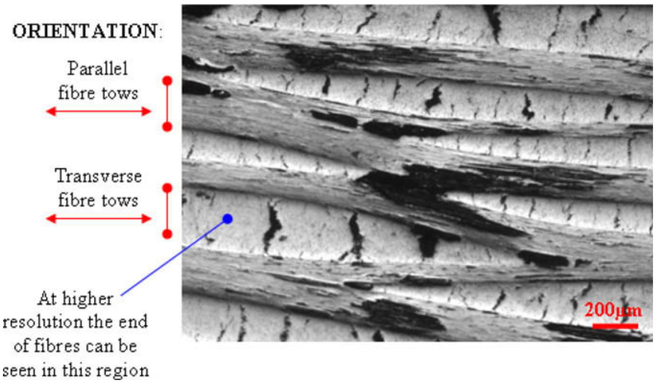

Fig. 3. Optical micrograph in the lamina orientation of the composite (graphitised).

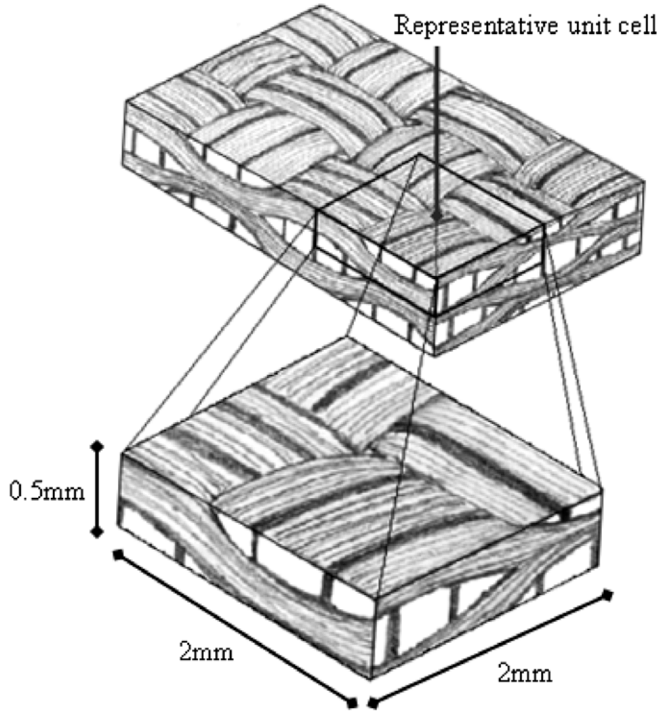

Fig. 4. Representative unit cell volume of the plain weave architecture (benchmark).

However, in these image-based meshes there were anomalous elements which caused discontinuities in the architecture. This was due to noise in the initially acquired tomographic data, which could not be removed despite the use of various filters and changes in imaging parameters.

3.2. 3D unit cell model

The unit cell FE model used for comparison was structured with dimensions from a series of observations and details through scanning electron micrographs [1,2]. It is based on plain weave fabric architecture of a representative volumetric cell, comprising of 186754 C3D4 (4-node linear tetrahedron) elements of ABAQUS software and represents ~0.5 × 2 × 2 mm of the composite volume. The shapes of elements were tetragonal as this gave best-fit and geometric conformity during meshing. This model was originally designed for thermal analyses and contained a jagged edge structure which did not affect thermal behavior [1]. However, for the current study the same FE model has been modified to a curvilinear shaped structure (Fig. 5), i.e., to avoid possible stress concentration effects at its edges under tension.

4. Experiments

4.1. Scanning electron microscopy

The Jeol JSM-6300 scanning electron microscope (SEM) was used to image the microstructures of the composites in secondary electron mode. Hence characterizing their complex woven architectures at a much higher resolution compared to the tomographic data. The composites were positioned in the venting chamber of the SEM and held in place by a press, while high vacuum was built, the accelerating voltage was set to 10 kV with the chamber closed and finally the electron beam activated. The composite surfaces were scanned and micrographs obtained.

4.2. Nanoindentation (input data)

The mechanical properties of the fiber and matrix constituents within the composites were determined by nanoindentation (Table 2) as it has been explained earlier in detail [7]. An MTS XP nanoindenter with a Berkovich diamond indenter was used to obtain transverse properties of the fibers, while a Hysitron Triboscope indenter system (Hysitron Inc., Minneapolis, USA) [20] with a diamond cubic corner tip, containing a corresponding atomic force microscope (AFM) was used to obtain longitudinal properties of the fibers and matrix properties. This was because the end-of-fiber regions that were indented for longitudinal properties were very small, i.e., ~5 μm in diameter. The MTS XP nanoindenter was used at a load range of 0–60 μN, while the Hysitron Triboscope indenter was conducted at a peak force of 5000 μN.

The Poisson's ratio used was 0.2 [21] and this has been retained for subsequent modeling. Since nanoindentation determines the near-surface mechanical properties of materials [22], it is important to evaluate the reliability of these data (Table 2) with regards to bulk properties reported in literature. These property data appeared suspicious for the fibers, particularly in the longitudinal direction, which were considerably lower than the values reported in the literature [23,24]. An assumption for this is that during indentation the longitudinal fibers may have separated under com-

Table 2
Indentation properties of the (a) graphitised and (b) un-graphitised composites [7]

Region indented	Number of indents	Mean modulus (GPa) to 1 d.p.
(a)		
Transverse fibers	11	7.1 (±1.6)
End-of-fibers	3	24.9 (±1.9)
Matrix	3	11.4 (±2.7)
(b)		
Transverse fibers	10	5.5 (±1.6)
End-of-fibers	3	22.8 (±1.9)
Matrix	3	7.5 (±2.7)

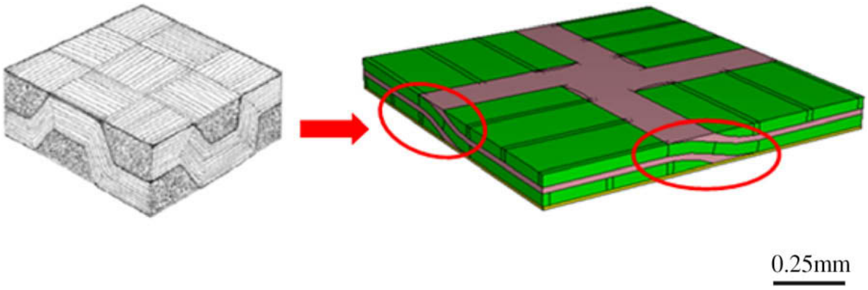

Fig. 5. Jagged edge unit cell modified to a curved structure for mechanical analysis.

pression, therefore, the stiffness could not be accurately measured. Furthermore, nanoindentation has been reported to only give the 'reduced' elastic modulus [25]. Thus, the mechanical properties used as input for the finite element calculations were 380 and 12 GPa [21,24], respectively, for the longitudinal and transverse directions of the fibers, while the data for the matrix were deemed acceptable.

4.3. Tensile tests

To validate FE predictions made by the image-based meshes and the unit cell, the Young's modulus in the lamina orientation of the composites were determined by tensile tests performed on an Instron Universal Testing Machine. Flat rectangular samples comprising of thickness ~4 mm, width ~10 mm and length ~50 mm were attached to two platens with two grippers. One platen was fixed and the other was moving at a rate of ~1 mm/min to apply loads up to 50 kN. An extensometer was also clipped onto the central section of the samples, allowing direct measurements of tensile strain without relying on cross-head displacement.

5. Results and discussion

5.1. Tensile test results

Experimental Young's modulus values for loading in the lamina orientation of the composites were obtained from experimental stress/strain plots of the graphitised and un-graphitised samples using lines of best-fit (Fig. 6). In Fig. 6, there is strong linear behavior in both composites. This is expected since similar trends have been reported earlier [26,27].

The graphitised composite exhibited a higher modulus value of ~77.5 GPa, while the un-graphitised composite exhibited ~71.2 GPa. This difference between the composites is due to their fabrication routes, where the graphitised composites have undergone graphitization at higher temperatures. During graphitization amorphous glass-like carbon is transformed to graphite. Carbonization of the thermosetting resins, used to make the non-graphitised glass-like carbon matrix, is accompanied by volume shrinkage. The fiber reinforcements restrict this shrinkage, thus inducing higher stresses within the composites at the interface between the fibers and matrix [15,28]. In summary, graphitization leads to a more compact, highly orientated and layered crystallographic structure, which is consequently much stiffer [24].

5.2. Image-based FE modeling

Image-based models were constructed for loading in the lamina orientation of the composites by setting specific boundary conditions to their cropped FE meshes. The aim was to re-create the experimental conditions of the tensile tests. These conditions involved fixing one face of the image-based mesh, while applying specific displacements to the opposing free face, i.e., based on the experimental strain limits in Fig. 6. This simulates the motion of the platens used to apply tensile loads. The FE meshes were subjected to a quasi-static analysis (static-load step) within ABAQUS CAE v6.6 EF-1.

5.3. Property assignment

Through observations of higher resolution images of the composite microstructures (Fig. 7), it is clear the image-based FE meshes did not have the resolution to pick-up the fine fiber architectures of the composites, e.g., the end-of-fiber regions. For this reason, elements representing the fibers and/or matrix could not be differentiated in the meshes. Therefore, the light grey elements as seen in Fig. 2 represent both fibers and matrix in one direction (say longitudinal) of the composite section, while the dark grey elements represent the other transverse direction.

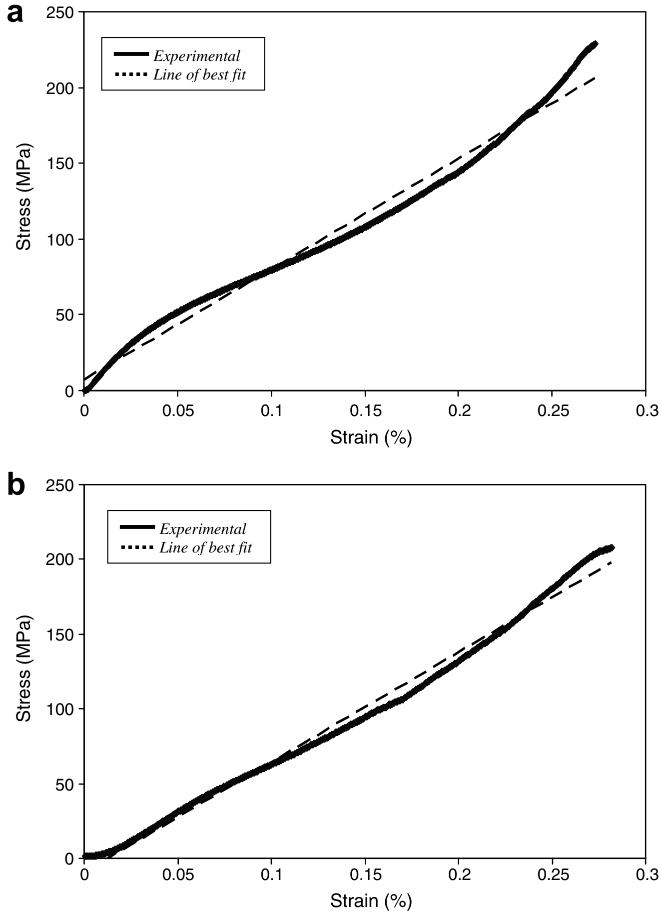

Fig. 6. Experimental stress/strain curves for tensile loading in the lamina orientations of the (a) graphitised and (b) un-graphitised composites.

To numerically model loading in the lamina orientations of the composites, orthotropic properties were assigned to these elements in their respective directions, using weighted mean values of the composite phases, i.e., via the 'rule of mixtures' [21]. The volume fractions of fibers, matrix and porosity within the composites have been determined earlier [7]. The input data used were the longitudinal and transverse mechanical properties of the fibers taken from literature [21,24], while the matrix properties were obtained by nanoindentation (Section 4.2). An assumption of 'even alignment' was also used (Fig. 8), since local orientation system could not be properly assigned to the woven profiles in the meshes due to discontinuities in the architecture caused by noise in the initial tomographic data.

5.4. Image-based results

The stresses and strains in the image-based FE models of the composites were analyzed by selecting elements of specific centre slices between the fixed and loaded faces of the models. Consequently, stress/strain contour maps were plotted (Fig. 9) and the Young's moduli predicted (Table 3). The elements in the centre of the models were chosen since strains during the experimental tensile tests were directly measured from the centre of the samples using a grip extensometer (Section 4.3). A unique feature of this

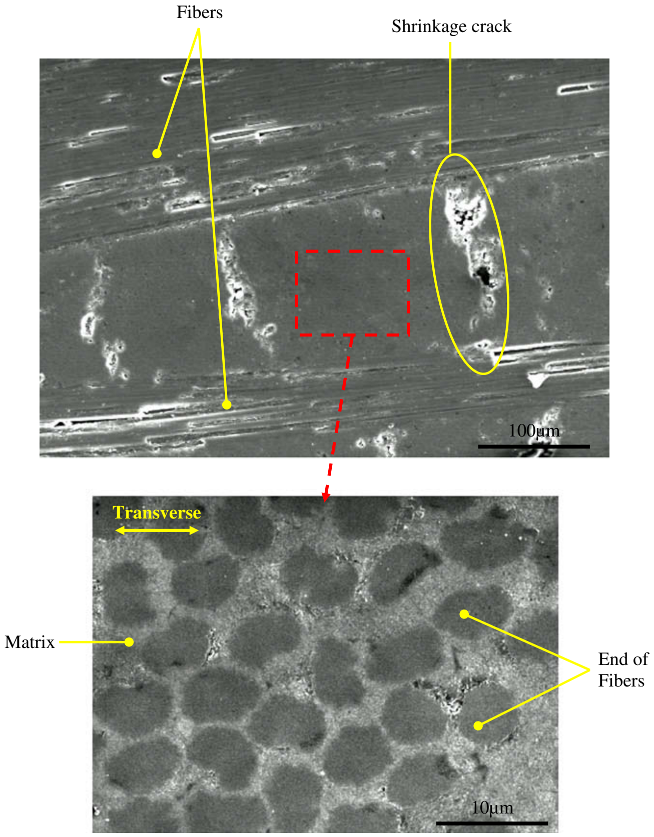

Fig. 7. SEM images of the composite microstructure, showing the end-of-fibers at higher resolution.

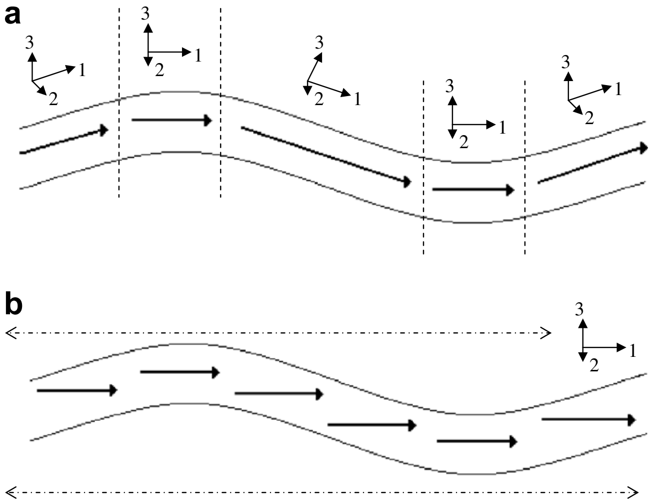

Fig. 8. Forms of property assignment (a) local coordinate systems accounting for undulating woven profiles (b) one global coordinate system assuming uniform or 'even' alignment.

image-based approach compared to prior unit cell methods [1–3] is that due to the presence of porosities in the model the characterization of stress effects around the different types of porosities could be characterized [2], even those within the 3D structure, which has always been difficult to do in the past.

The plotted stress/strain contour maps showed regions in the samples where higher localized stresses had accumulated due to the presence of pores. Examples of this have been highlighted in Fig. 9(b). The results for loading in the lamina orientation of the composites indicated that the image-based models showed strong agreement with experimental data, particularly for the un-graphitised sample (Table 3). The improved agreement for the un-graphitised material could be due to the volume sampled in the analysis. The strong agreement of the experimental with the numerically modeled values demonstrates the validity of these numerical models in this orientation.

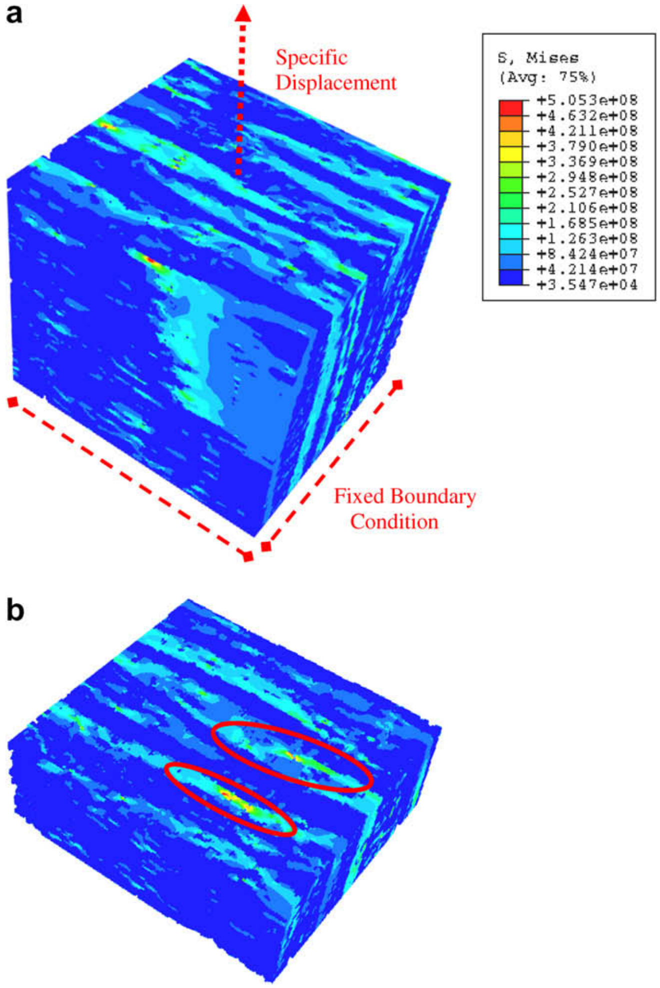

Fig. 9. (a) Stress/strain contour maps for loading in the lamina orientations of the image-based FE models (graphitised) and (b) porosity effects within the 3D structure.

Table 3
Experimental results compared to image-based and unit cell FE predictions for Young's modulus, E, in the lamina orientations of the composites

Modulus results (GPa)	Graphitised composite	Un-graphitised composite
Experimental	77.5	71.2
Image-based FE model	74.2 (−4.3%)	72.0 (+1.1%)
Unit cell FE model	85.0 (+9.7%)	70.0 (−1.7%)

Percentage errors are shown in parenthesis.

5.5. Unit cell FE modeling

The unit cell model adopted for comparison was based on the same FE analysis used for the image-based models, while the finer architectures of the composites were considered, and orthotropic properties assigned to the fiber tows fully accounting their woven profiles, while the matrix remained isotropic. As stated earlier in Section 2, the directions of fibers in the lamina orientations of the composites were both longitudinal and transverse. This has been highlighted in the plotted stress/strain contour maps of the unit cell (Fig. 10), where clear differences are seen in the fiber tow regions positioned longitudinal (*X*) and transverse (*Y*) to the applied load. The longitudinal fibers have generated greater stresses due to having higher Young's modulus values aligned, as deduced earlier in Table 2.

The stresses appeared higher in specific areas of the image-based model (Fig. 9) than in this unit cell model. This is because the image-based model contained porosity and considered the actual surface topography of the composite, which can enhance localized stresses during tension [24]. The predictions made using the unit cell model are also listed in Table 3. The results indicate that this 3D unit cell model presented less convincing predictions compared with experimental results in contrast to the image-based models. This comparison is further discussed next.

5.6. Discussion of FE results

The overall results show that the image-based models for measuring the tensile Young's moduli of the composites through loading in the lamina orientation, gave better agreement with experimental results than the unit cell model (Table 3). The agreement was exceptional for the un-graphitised material, in which the difference was only +1.1%, while for the graphitised material it was a respectable −4.3%. The predictions made using the unit cell model were also very strong for the un-graphitised material, where the difference was only −1.7%, and for the graphitised material it was +9.7%, which is still reasonable.

On comparing the two composite materials, the results for both model types are better for the un-graphitised sample. This is partly dependent upon the input data used, since nanoindentation was found to be unreliable for the carbon fiber constituents (Section 4.2). This improved agreement indicates that the micro-mechanical properties used from literature [21,24] were better suited to the un-graphitised material, especially since the same unit cell model was used for both composites.

The major difference between the models is seen in the graphitised sample, where the image-based model under-predicted, unit cell model significantly over-predicted the values. This is supported by their stress/strain contour maps (Figs. 9 and 10), in which the image-based model contains specific areas of higher localized stresses due to porosity, while the overall distribution of stresses are still higher in the unit cell model. The microstructural differences between the two models were the consideration of the finer architectures of the composites and porosity. The image-based approach highlighted true porosity in its structure formed directly from X-ray tomographic data, although the fiber tows and matrix could not be differentiated in the mesh (Section 5.4). In comparison, the unit cell model was based solely on idealizations of the composite microstructure, in which porosity was neglected. Compensation has been done for this discrepancy in the unit cell by sequential sub-modeling of different porosities for the individual's property degradation effect on the bulk thermal properties [1].

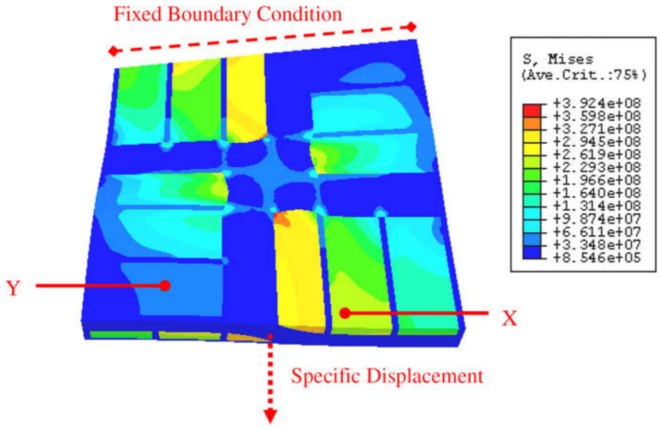

Fig. 10. Stress/strain contour map for loading in the lamina orientation of the unit cell (graphitised).

In summary, it would be fair to conclude that actual representations of the composite materials (the image-based approach), despite some ambiguities, produce better numerical models than simple idealizations of the composite microstructure in 3D unit cell models. It is not truly valid to assume that such materials can be represented reliably by an infinitely repeating, ideal structure, since they have complex architectures and are difficult to fabricate. However, in the case of the un-graphitised material, where both model types were found to be strong and the difference insignificant (Table 3), it could be argued that the unit cell model should be the preferred option for this composite. This is because the model is much easier to create [1] and requires lower computational effort. Furthermore, the image-based model has the added costs of acquiring quality scan data using the X-ray microtomography kit [7], as well as cost of licensing Simpleware® software [10].

6. Conclusions and summary

A methodology in creating the image-based FE meshes from X-ray microtomography data sets of two nuclear 2D woven C/C composites was devised [7,12]. This involved defining the image greyscale thresholds of the composite phases that represented the volume fraction of each phase in the mesh. Nanoindentation was applied to determine the stiffness of these phases. It was found that the fibers exhibited more elastic recovery than the matrix. Furthermore, the indentation properties of the fibers were found to be lower than bulk properties reported in the literature. The matrix properties were however deemed adequate as input data for the FE analysis to model (numerically) the tensile behavior of the composites.

A 3D unit cell FE model of the structure was also adopted for comparison [1,2]. Both model types were then subjected to FE analyses to model the Young's moduli of the composites. The image-based FE models were found to give better agreement with experimental results compared to the unit cell models. The major advantage of the image-based approach was the characterization of actual porosity.

In conclusion, a quantum step forward in the modeling of complex architectures has been demonstrated in the image-based approach. The main achievements have been:

- A realistic expectation in modeling the irradiated behavior of advanced composite materials, since previous attempts have neglected the actual porosity within such materials. The changes in porosity for ceramic materials during irradiation are known to be detrimental [29,30].
- A comprehensible cost cutting measure in developing new materials for extreme environments (ExtreMAT), given that representative models provide an accurate way in predicting the likely performance of a composite before actually embarking an expensive testing process.

References

[1] J.K. Farooqi, M.A. Sheikh, Compos. Mater. Sci. 37 (2006) 361.
[2] P. Del Puglia, M.A. Sheikh, D.R. Hayhurst, Composites Part A 35 (2004) 223.
[3] E.J. Barbero, T.M. Damiani, J. Trovillion, Int. J. Solids Struct. 42 (2005) 2489.
[4] D. Scida, Z. Aboura, M.L. Benzegagh, E.A. Bocherens, Compos. Sci. Technol. 59 (1999) 505.
[5] K.M. Entwistle, Basic Principles of the Finite Element Method, IOM Communications Ltd., London, 1999.
[6] M. Alenius, Finite Element Modelling of Composite Bridge Stability, MSc Thesis, Royal Institute of Technology, Department of Mechanics, Stockholm, 2003.
[7] J. Ali, C. Berre, P.M. Mummery, Energy Mater. 1 (2006) 179.
[8] T.J. Marrow, J.Y. Buffiere, P.J. Withers, G. Johnson, D. Engelberg, Int. J. Fatigue 26 (2004) 717.
[9] L. Babout, P.M. Mummery, T.J. Marrow, A. Tzelepi, P.J. Withers, Carbon 43 (2005) 765.
[10] Simpleware® Ltd., Innovation Centre, Rennes Drive, Exeter, EX4 4RN, UK.
[11] ABAQUS CAE v6.6 EF-1 (2007), ABAQUS/CAE, ABAQUS Inc., Rhode Island, USA.
[12] J. Ali, P.M. Mummery, in: Proceedings, Seventh IEA International Workshop on SiC/SiC Composites for Fusion and Advanced Fission Applications, September 2006, Petten, Holland, NRG.
[13] S. Youssef, E. Maire, R. Gaertner, Acta Mater. 53 (2005) 719.
[14] P. Babin, G. Della Valle, R. Dendievel, N. Lassoued, L. Salvo, J. Mater. Sci. 40 (2005) 5867.
[15] C. Berre, S.L. Fok, B.J. Marsden, L. Babout, A. Hodgkins, T.J. Marrow, P.M. Mummery, J. Nucl. Mater. 352 (2006) 1.
[16] O. Amsellem, K. Madi, F. Borit, D. Jeulin, V. Guipont, M. Jeandin, E. Boller, F. Pauchet, J. Mater. Sci. 43 (2008) 4091.
[17] D. Ulrich, B. Van Rietbergen, A. Laib, P. Ruegsegger, J. Biomech. 32 (1999) 821.
[18] P. Magne, Dent. Mater. 23 (2007) 539.
[19] J.D. Wolodko, Z. Xia, F. Ellyin, Mater. Sci. Technol. 16 (2000) 837.
[20] Hysitron Inc., 10025 Valley View Road, Minneapolis, MN 55344, USA.
[21] D. Hull, T.W. Clyne, An Introduction to Composite Materials, second ed., Cambridge University Press, 1993.
[22] D.T. Marx, L. Riester, Carbon 37 (1999) 1679.
[23] C.R. Thomas, Essentials of Carbon–Carbon Composites, Royal Society of Chemistry, Cambridge, 1993.
[24] K.K. Chawla, Ceramic Matrix Composites, Chapman & Hall, 1993.
[25] M. Zhao, C. Jiang, S. Li, S.X. Mao, Mater. Sci. Eng. A 409 (2005) 223.
[26] B.N. Cox, G. Flanagan, Handbook of Analytical Methods for Textile Composites, Contractor Report, National Aeronautics and Space Administration (NASA), USA, 1997.
[27] P.B. Pollock, Carbon 28 (1990) 717.
[28] F.A. Quli, P.A. Thrower, L.R. Radovic, Carbon 36 (1998) 1623.
[29] K. Hamada, S. Sato, A. Kohyama, J. Nucl. Mater. 212–215 (p-2) (1994) 1228.
[30] S. Blazewicz, J. Piekarczyk, J. Chlopek, J. Blocki, J. Michalowski, M. Stodulski, P. Zychowski, Carbon 40 (2002) 721.